Author(s): Sternberg, M. & Kaukonen, M. & Nieminen, Risto M. & Frauenheim, Th.

Title: Growth of (110) diamond using pure dicarbon

Year: 2001

Version: Final published version

Please cite the original version:

Sternberg, M. & Kaukonen, M. & Nieminen, Risto M. & Frauenheim, Th. 2001. Growth of (110) diamond using pure dicarbon. Physical Review B. Volume 63, Issue 16. 165414/1-9. ISSN 1550-235X (electronic). DOI: 10.1103/physrevb.63.165414.

Growth of (110) diamond using pure dicarbon

M. Sternberg,[1,*] M. Kaukonen,[2] R. M. Nieminen,[2] and Th. Frauenheim[1]
[1]*Department of Physics, Theoretical Physics, University of Paderborn, D-33098 Paderborn, Germany*
[2]*Laboratory of Physics, Helsinki University of Technology, P. O. Box 1100, FIN-02015, Finland*
(Received 5 October 2000; revised manuscript received 19 December 2000; published 3 April 2001)

We use a density-functional-based tight-binding method to study diamond growth steps by depositing dicarbon species onto a hydrogen-free diamond (110) surface. Subsequent C_2 molecules are deposited on an initially clean surface, in the vicinity of a growing adsorbate cluster, and finally near vacancies just before completion of a full new monolayer. The preferred growth stages arise from C_{2n} clusters in near ideal lattice positions forming zigzag chains running along the $[\bar{1}10]$ direction parallel to the surface. The adsorption energies are consistently exothermic by 8–10 eV per C_2, depending on the size of the cluster. The deposition barriers for these processes are in the range of 0.0–0.6 eV. For deposition sites above C_{2n} clusters the adsorption energies are smaller by 3 eV, but diffusion to more stable positions is feasible. We also perform simulations of the diffusion of C_2 molecules on the surface in the vicinity of existing adsorbate clusters using a constrained conjugate gradient method. We find migration barriers in excess of 3 eV on the clean surface, and 0.6–1.0 eV on top of graphenelike adsorbates. The barrier heights and pathways indicate that the growth from gaseous dicarbon proceeds either by direct adsorption onto clean sites or after migration on top of the existing C_{2n} chains.

DOI: 10.1103/PhysRevB.63.165414 PACS number(s): 81.15.Aa, 61.43.Bn, 81.05.Tp

I. INTRODUCTION

The growth of ultrananocrystalline diamond (UNCD) films from C_2 precursors produced by C_{60} fragmentation in hydrogen-poor plasmas[1–3] has recently attracted attention because of the high growth rates and resulting good mechanical and electronic properties of the films. Diamond films in general are attractive for a broad range of applications like tool coatings, electrochemical electrodes, heat spreaders, IR-transmissive windows, and electron emitters. The physical properties of these films, which are mainly determined by their microstructure, must be tuned for each of these applications. Conventional diamond films as grown from H/CH_3 mixtures are characterized by crystallites in the micrometer size range. In several recent experiments[4–6] it was confirmed that the addition of argon to the plasma allows continuous control over the crystallite size. Most importantly, at argon concentrations in a narrow window around 95%, the resulting films are ultrananocrystalline with a typical crystallite size of just 3–10 nm. The resulting films exhibit a smooth surface and a uniform morphology throughout the film, which has a thicknesses of at least 20 μm. The films are found to be hard, have low friction, and are wear resistant.[2,7,8] The small size of the crystallites implies that a relatively high percentage (up to 10%) of all atoms are located at grain boundaries, where they are π bonded[9,10] and contribute to electrical conductivity. The UNCD films thus exhibit a combination of useful properties typical for diamond films supplemented by electrical conductivity and electron emissivity,[11] which makes them very attractive for device applications.

There is evidence that the growth proceeds mainly on the (110) face.[12] Previous studies[13,14] explored initial growth stages with dicarbon on the hydrogen-terminated (110) face without hydrogen abstraction by way of insertion of C_2 into C-H bonds on the surface. The presence of C_2 near the surface during growth and its likely contribution to the growth process have been confirmed experimentally through characteristic intense Swan-band radiation in both microwave plasma chemical vapor deposition[4,5] and hot-filament chemical vapor deposition.[6] In the present work, we consider deposition steps onto the clean diamond (110) surface without hydrogen participation. Starting out from a clean surface we investigate the local atomic configuration arising from the adsorption of a C_2 molecule. Subsequently, more C_2 molecules are deposited in the vicinity of a previous adsorbate cluster. By comparing the total energy of these structures, we identify preferred growth stages as those arising from C_{2n} clusters in the form of zigzag chains running along the $[\bar{1}10]$ direction parallel to the surface.

We also perform simulations of the diffusion of C_2 molecules on the surface in the vicinity of existing adsorbate clusters using a constrained minimization technique.[15–17] The barrier heights and pathways indicate that the growth from gaseous dicarbons proceeds either by direct adsorption onto clean sites or after migration above existing C_{2n} chains.

The computational method is briefly outlined in Sec. II. In Sec. III, the properties of clean diamond (110) surfaces are calculated using a density-functional-based tight-binding method and compared with more elaborate *ab initio* results. The initial adsorption steps for diamond growth are studied in Sec. IV, followed by an evaluation of diffusion barriers for C_2 on diamond (110) in Sec. V. We then analyze some molecular dynamics trajectories in Sec. VI. Finally, we present conclusions in Sec. VII.

II. COMPUTATIONAL METHOD

In performing our atomistic simulations, we apply the density-functional-based tight-binding (DFTB) method.[18] In order to correctly take into account effects of surface polarization we have used the self-consistent charge extension of

the method.[19] It has been applied successfully to diamond systems including studies of surfaces and diffusion problems.[20,21] It reproduces total energy differences between various carbon bulk structures within 50–100 meV/atom compared to *ab initio* calculations (Refs. 18 and 22). For surface related effects, the errors are determined to be less than 0.2 eV/atom.

The surfaces are simulated using a two-dimensional slab-geometry with varying thickness. The bottom layer is saturated by a fixed monolayer of pseudohydrogen atoms which do not mutually interact. The lateral extent of the cell varies from 3×3 unit cells up to 8×3 unit cells, where the bigger extent is along the chain direction. This direction is assigned as the x axis. For all atomic structure calculations, we used the Γ-point approximation to sample the Brillouin zone, which amounts to a $\boldsymbol{k}$-point sampling with as many points as real-space unit cells. We let the atoms relax in a conjugate gradient scheme.

The diffusion and adsorption runs are done using a constrained conjugate gradient method. The forces during the conjugate gradient minimization are modified by the method described by Ciccotti *et al.* and by Ryckaert.[15–17] The center of mass of the C_2 molecule is moved in a given direction with steps of 0.1 Å. Because the constraint is to the center of mass movement, the C_2 may rotate or dissociate freely.

III. CLEAN DIAMOND (110) SURFACE

The clean (110) surface of diamond as obtained from bulk cleavage has one dangling bond per atom pointing at an angle of 19.5° away from the surface normal. The atoms are arranged in zigzag chains flat on the surface directed along the $[\bar{1}10]$ direction.

For initial studies we used six bulk monolayers of carbon. We find that only negligible relaxations take place in the lower two layers and therefore we use only four carbon monolayers for the remaining calculations. The applicability of this size of supercell is tested by comparing the minimum energy geometries of a C_4 adsorbate on the (110) surface with supercells consisting of four and six monolayers, respectively. The comparison between fully relaxed structures calculated with both numbers of monolayers yields very small differences in the atomic positions of about 0.015 Å in both the lateral and vertical positions of all corresponding atoms, including those of the adsorbate.

There has been some controversy in the literature about whether the C(110) surface reconstructs or not.[23,24] We find here a symmetric flat (1×1) surface in agreement with *ab initio* studies[25] and experiments.[26] The upper surface layer moves inward by $\Delta z_1=-0.16$ Å, and the next layer outward by $\Delta z_2=0.02$ Å. The chains in the top layer are slightly straightened by a relaxation of 0.1 Å toward the chain axis, resulting in a bond angle of 122.0° and a bond length of 1.44 Å. This geometry is in excellent agreement with the *ab initio* results in Ref. 25, summarized in Table I. Taking into account the 0.015 Å offset in the equilibrium bulk bond length d_0, all bond lengths agree within 0.01 Å, or 0.6% of d_0.

TABLE I. Calculated geometry of the clean relaxed C(110) surface. Following the notation of Ref. 25, d_{ij} is the bond length between atoms of the ith and jth layers; d_0 is the equilibrium bulk bond length, and θ_i is the bond angle within layer i. Δy_i and Δz_i are the relaxation of the atomic positions in layer i along the y ([001], transversal to chains) and z ([110], surface normal) directions, respectively. The units are Å and degrees, respectively.

	Ref. 25		This work	
d_0	1.529	(100%)	1.544	(100%)
d_{11}	1.419	(−7.2%)	1.441	(−6.7%)
d_{12}	1.467	(−4.1%)	1.490	(−3.5%)
d_{22}	1.490	(−2.6%)	1.505	(−2.6%)
d_{23}	1.576	(+3.1%)	1.587	(+2.7%)
d_{33}	1.526	(−0.2%)	1.542	(−0.2%)
θ_1	123.3		122.0	
θ_2	113.8		113.8	
Δy_1	±0.10		±0.10	
Δz_1	−0.17		−0.16	
Δy_2	±0.03		±0.00	
Δz_2	+0.03		+0.02	

IV. ADSORPTION AND ENERGETICS OF SMALL CARBON CLUSTERS ON (110) DIAMOND

The energetically most favorable cluster configurations after repeated C_2 additions are summarized in Fig. 1 up to C_8 on (110). In the following, a more detailed description of the surface cluster geometries will be given.

A. Initial C_2 deposition

In order to sample the energy landscape above the clean (110) diamond surface for C_2 adsorption we place a C_2 molecule in a vertical orientation near the surface on a hexagon-like set of points above the atoms and bond centers of the two topmost monolayers. By symmetry, only seven positions remain unique. The lower atom of the molecule is placed about 2 Å away from the nearest surface atom. A conjugate gradient relaxation from each of the lateral starting positions shows that the molecule is either reflected from or adsorbed onto the surface. The reflections occur for starting positions directly above the atoms and bonds of the top monolayer. From all of the starting positions not directly above a top-layer chain the C_2 molecule is bonded and forms a bridge above the ''trough'' between two adjacent top-layer chains. The deposition proceeds in two stages (see Fig. 2).

Initially, the C_2 sticks with one end to the nearest surface atom with an inclination of about 45° to the surface normal. There is a very low energy barrier of order 0.1 eV towards the final adsorption stage in which the molecule bonds symmetrically in an orientation corresponding to the diamond lattice. At this final stage, both adsorbate atoms are 1.0 Å above the top monolayer and are threefold coordinated with a bond length of 1.38 Å between them. Each adsorbate atom forms two bonds toward the surface, one bond corresponding to the diamond lattice with a length of 1.49 Å, the other being a stretched bond of 1.91 Å toward the adjacent atom

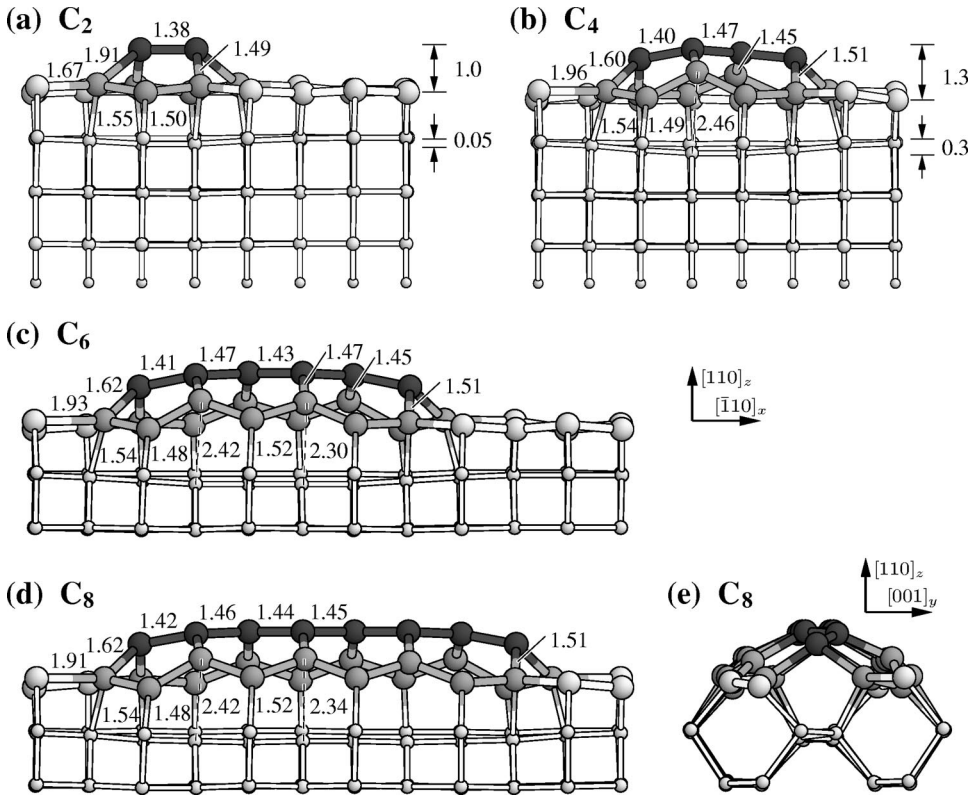

FIG. 1. Overview of relaxed structures from subsequent depositions of C_2 molecules onto a clean diamond (110) surface. (a) C_2, (b) C_4, (c) C_6, (d) C_8, all along the $y=[001]$ direction, and (e) C_8, along the $x=[\bar{1}10]$ direction. The numbers given are distances in Å. Atoms of the adsorbate and the surface layer are shown bigger. Dark atoms indicate the adsorbate cluster, medium gray atoms its first and ring-forming second neighbors within the surface layer, and lighter gray are other atoms. Small spheres at the bottom indicate hydrogen saturation. For (c)–(e), only partial models are shown.

in the same surface chain [see Fig. 1(a)]. The result is the formation of two fivefold rings with a common bond formed by the adsorbed molecule. There is a slight lateral pinch contraction of the surface monolayer. All its atoms remain bonded to the subsurface, which is indented below the adsorbate by about 0.05 Å.

The binding energies of the C_2 molecule to the clean (110) surface are fairly high, as can be seen in the fifth column of Table. II. The energy gain is mainly the result of forming four bonds to the surface, which yields about 2 eV for each bond; this is plausible considering its similarity to the atomic binding energy of 2.3 eV/bond as obtained by the DFTB method for bulk diamond. Breaking the initial triple bond within the C_2 molecule and the stretch of surface bonds near the adsorbate offsets the result to give the adsorption energy of 8.1 eV, listed in the table.

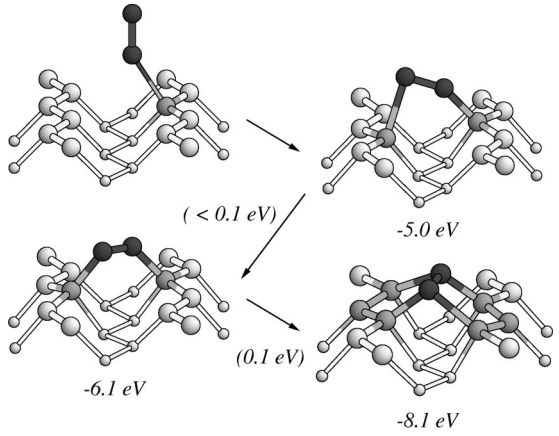

FIG. 2. Initial steps for deposition of a C_2 molecule onto a clean diamond (110) surface. The energies are given relative to a clean surface and a distant C_2. Energies in parentheses indicate barriers. Atom designation is the same as in Fig. 1.

B. Addition of C_2

As a next step, we studied the effect of adding another C_2 molecule near an existing C_2 adsorbate. Obviously, the deposition onto a site more than one surface lattice spacing away from the initial adsorbate results in two isolated clusters of similar configuration as discussed above, unless a topological mismatch prevents the completion of the ring formation for a nearby site, as shown in Fig. 3(a). In this case, the strain field introduced by the second adsorbate results in a bond switch for one of the backbonds, with an accordingly high adsorption energy of -7.2 eV. For deposition onto a site of the neighboring chain, the geometry and energy are essentially the same as for the isolated case [see Fig. 3(b)]. We note that in this case the low barriers found in the initial adsorption process are no longer present, probably due to the small local strain field induced. This effect supports the idea of a rapid spread of such C_2 adsorption sites across the surface.

C. C_4 clusters

The highest gain in energy for the second C_2 deposition is obtained at a site directly above the first C_2 molecule [see Figs. 1(b) and 4]. The second molecule bonds at the neighboring diamond-lattice site along the $[\bar{1}10]$ valley, in a diamondlike configuration next to the first one, and forms a

TABLE II. Energy barriers (E_{barr}) and adsorption energies (E_{ads}) of C_2 (and C) at the initial and final stages of growth, for varying target sites. The ''top'' position means that the initial position of the C_2 is above a C_{2n} cluster; ''end'' refers to an initial C_2 position above the edge along the $[\bar{1}10]$ direction of the C_{2n} cluster; ''same'' and ''other'' express whether the added C_2 is above the same or the adjacent (110) trough as the existing C_{2n} cluster on the surface. Negative indices indicate missing C atoms in an otherwise continuous chain or on the (110) surface.

Initial configuration	Final configuration	Figure	E_{barr} (eV)	E_{ads} (eV)	E_{ads} (eV) (Ref. 14)
C_2+(110)	(110):C_2	Figs. 1(a), 2	0.1	−8.1 [a]	−7.8
C_2+(110):C_2 top	(110):C_4	Figs. 1(b), 4	0.1	−10.3 [a]	−8.8
C_2+(110):C_2 same	(110):C_2,C_2 same	Fig. 3(a)	0.2	−7.2	
C_2+(110):C_2 other	(110):C_2,C_2 other	Fig. 3(b)	0.0	−8.3	−7.8
C_2+(110):C_4 end	(110):C_6	Fig. 1(c)	0.1	−9.6 [a]	
C_2+(110):C_4 top	(110):C_4,C_2		0.7	−6.5	
C_2+(110):C_6 end	(110):C_8	Fig. 1(d)	0.5	−8.8 [a]	
C_2+(110):C_6 top	(110):C_6,C_2	Fig. 5(b)	0.0	−2.0	
C_2+(110):C_6 top	(110):C_8 defect	Fig. 5(c)	1.8	−4.9	
C_2 + (110):C_6 other	(110):C_6,C_2 other		0.0	−7.8	
C_2+(110):(2×1):C_{-3}	(110):(2×1):C_{-1}	Fig. 6(b)	0.6	−6.3	
C_2+(110):(2×1):C_{-2}	(110):(2×1)	Fig. 6(d)	0.3	−10.2 [a]	
C_2+(110):(2×1)	(110):(2×1):C_2	Fig. 7	0.0	−7.2	
C_2+(110):C_{-3}	(110):C_{-1}		0.5	−6.9	
C_2+(110):C_{-2}	(110)		0.4	−8.1	
C_2+(110):C_{-1}	(110):C		0.0 [b]/2.6	−6.8 [b]/−8.3	
C+(110):C_{-1}	(110)		0.0	−10.4	

[a] C_{2n} chain growth and coalescence processes.
[b] Metastable state.

four-atom-long zigzag chain which amounts to a seed for the next monolayer. At the ends of the new chain, fivefold rings are formed similar to the ones in the C_2 case. The ridge of the adsorbate is a z-shaped symmetric chain of three bonds with lengths of 1.40 Å at the ends and 1.47 Å in the center. The central two atoms are raised 1.3 Å above the top monolayer, which corresponds to a slightly outward relaxation with respect to the ideal lattice sites. The end atoms are 0.3 Å closer to the surface. The center bond is the common

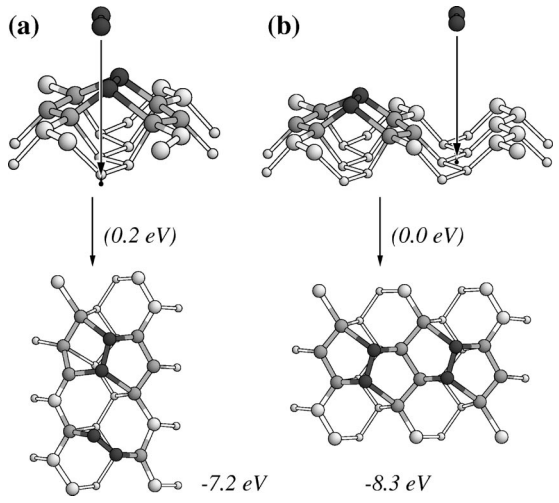

FIG. 3. Continued deposition of a C_2 molecule onto a diamond (110) surface on sites next to an existing C_2 adsorbate. The targeted neighboring site is (a) along the $x=[\bar{1}10]$ direction, and (b) along the $y=[001]$ direction. The total energies are given relative to initially separated components. Energies in brackets indicate barriers. Atom designation is the same as in Fig. 1. Additional small markers indicate the target location.

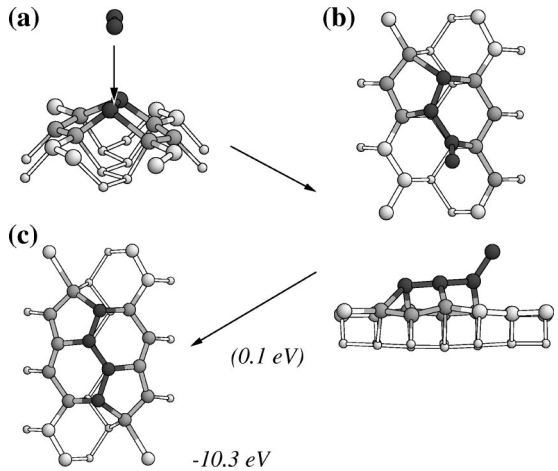

FIG. 4. Continued deposition of a C_2 molecule onto a diamond (110) surface on top of an existing C_2 adsorbate, with the transition state shown from the top and side. The resulting adsorbate cluster is topologically similar to a C_{60} fragment. The panels show (a) the initial, (b) the transition, and (c) the final state. The total energies are given relative to initially separated components. Atom designation is the same as in Fig. 1.

side of two adjacent sixfold rings connecting the new chain to the surface monolayer. Topologically, the rings supporting the C_4 adsorbate above the surface form a pyracylene structure, which is the basic structural element of a C_{60} fullerene. A local pinch contraction of the surface monolayer occurs as in the previous case. However, the outer bonds of the adsorbate are here, at 1.6 Å, closer in length to actual bonds, at the expense of the transition to the uncovered parts of the surface, for which the bonds are now stretched to a distance of 1.9–2.0 Å. Furthermore, we observe the breaking of backbonds in the middle of the aggregate, resulting in a cluster of sp^2-like coordinated atoms arranged in a domelike configuration. The similarity to such a highly stable configuration as a fullerene explains the fact that this C_4 cluster represents the highest energy gain for an approaching C_2 molecule among the structures considered in Table. II.

D. C_6 and C_8 clusters

The next C_2 adsorption to the C_4 pyracylenelike adsorbate results in a C_6 adsorbate, shown in Fig. 1(c), with an adsorption energy of 9.6 eV. Further C_2 adsorption yields an adsorption energy of 8.8 eV and a surface C_8 cluster, shown in Fig. 1(d). Thus, the energy gain is at least 8 eV for the repeated C_2 surface chain addition as shown up to C_8 on the surface. We expect the adsorption gain to level off at about 8.5 eV for longer chains.

The C_6 adsorbate has four sixfold rings in the middle and a fivefold ring at each end. The C_8 adsorbate is essentially identical to it, but has of course two more sixfold rings along its length. As in the case of the C_4 adsorbate, the underlying substrate atoms are raised above the surface and flattened to sp^2-like coordination together with the adsorbed atoms.

E. Adsorption barriers

The energy barriers for C_2 adsorption (Table II, fourth column) are either zero or very low. The highest energy barrier in the case of C_2 addition at the end of C_8 is probably a finite size effect.

The initial C_2 addition at a diamond site in a ''valley'' on the surface makes the bonds shorter in the neighboring ''valley.'' This makes the adsorption of an additional C_2 easier at the neighboring ''valley'' at a diamond site, as can be seen by comparing the energies in the third and fourth rows in Table II.

F. Surface defect formation

There is a metastable energy minimum when adsorbing a C_2 molecule on the top of C_4 or C_6 adsorbates (rows 6 and 8 in Table II). In the metastable state (C_2+C_{2n}) one of the C_2 atoms is singly bonded to the surface C_{2n} complex [see Fig. 5(b)]. The bonded C_2 is only 2.0 eV lower in energy than free C_2. We believe this metastable minimum configuration plays a key role in the growth of (110) diamond. It enables the diffusion of the C_2 molecule to the end of an existing growing C_{2n} complex in the diamond configuration. If the C_2 molecule is forced deeper onto a C_6, there is another metastable minimum energy structure consisting of one seven-membered ring, one six-membered ring and six five-membered rings (row 9 in Table II). The energy gain from the gaseous C_2 to this non-diamond-growth favoring configuration is 4.9 eV and the energy barrier toward the final metastable minimum is 1.8 eV. We believe that similar metastable defect structures form when a C_2 adsorbs on C_{2n} with too high kinetic energy, approximately $E_K > 3-5$ eV, taking into account kinetic contributions to the energy barriers.

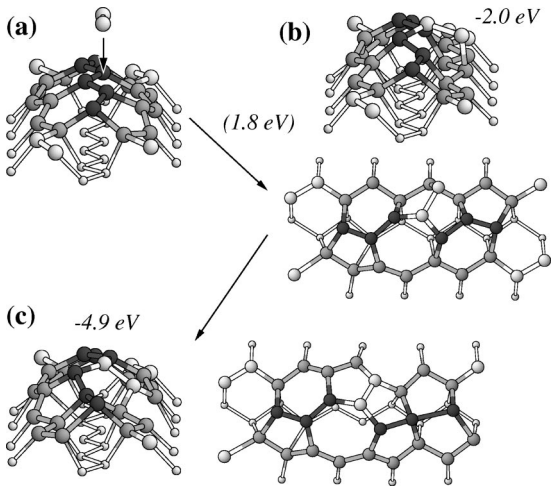

FIG. 5. Continued deposition of a C_2 molecule onto a diamond (110) surface over a C_6 adsorbate with high insertion energy. The panels show (a) the initial, (b) the transition, and (c) the final state. The total energies are given relative to initially separated components. Atom designation is the same as in Fig. 1, with the added C_2 molecule shown in white.

G. Surface vacancy filling

When the growth proceeds further, different C_{2n} clusters along the same (110) surface trough will eventually meet and coalesce. Given that growth proceeds by C_2 addition, the critical stage is reached just before coalescence, when there will be a gap between two cluster ends corresponding to either three or two missing atoms. Assuming the clusters are seeded at random sites, both cases have equal probability but quite different energetics for subsequent C_2 additions.

In either case we see the approaching C_2 first in a metastable bridging configuration from a chain end to a bare surface site, and directly between the two chain ends, for the three- and two-site-wide gap, respectively [see Figs. 6(a) and 6(c)]. Both added atoms remain just twofold coordinated. After overcoming barriers of 0.6 eV and 0.3 eV, respectively, the adsorbate extends the existing C_{2n} chain by another atom pair [see Figs. 6(b) and 6(d)].

For the original three-atom gap, a single-atom vacancy remains next to a still just two-fold coordinated atom. Accordingly, the gain in adsorption energy is rather low at 6.3 eV. However, the remaining single-atom gap remains reactive, and may be filled at a later stage.

The two-atom gap yields a much higher adsorption energy of 10.2 eV, comparable to the high gains found in the initial adsorption stages. The final stable configuration is a continuous chain with broken backbonds for atoms on either side of

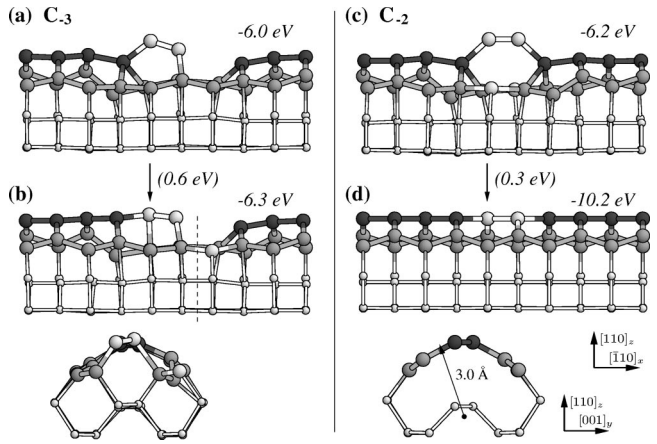

FIG. 6. Final stages of $[\bar{1}10]$ chain growth and coalescence on a diamond (110) surface: (a) and (b) for a three-site vacancy, (c) and (d) for a two-site vacancy. Panels (a) and (c) show the metastable adsorption phases, and panels (b) and (d) the relaxed minimum configuration. Atom designation is the same as in Fig. 1, with the added C_2 molecule shown in white. The total energies are given relative to initially separated substrate and added C_2. Energies in parentheses indicate barriers. The dashed line in (b) indicates a cut used for the alternative view along $[\bar{1}10]$ in this panel. The arrow in (d) indicates an empirical bending radius for the graphene sheet.

the top ridge. This structure is a bent graphene sheet with a bending radius of about 3 Å. Before discussing its properties in the next chapter, we briefly sketch the other variants for surface vacancy filling.

For the final stage of surface coalescence, we considered a nearly complete surface monolayer, with up to three consecutive atoms along the $[\bar{1}10]$ direction removed. The filling of these surface vacancies results in energy gains between 6.9 and 10.4 eV, as listed in the last rows of Table II. The filling of the last single-atom vacancy can take place either by a single C atom adsorption at the vacancy, with an energy gain of 10.4 eV without a barrier, or by a C_2 addition process, which has a rather high barrier from a metastable minimum at a gain of 6.8 eV to its completion at 8.4 eV. Furthermore, it leaves a singly bonded C atom on an otherwise perfect (110) surface. The energy required to desorb the extra C atom is of order 8 eV.

H. Graphitization and rebonding

As shown in the preceding sections, the growth by the C_2 chain addition mechanism will eventually lead to coalescing chains, with broken backbonds on either side. In order to investigate the consequences of the broken backbonds for the surface stability during growth we have generated and relaxed a model in which every other trough along $[\bar{1}10]$ was covered with a continuous chain, resulting in a C(110):(2 $\times$1) reconstruction, shown in Fig. 7(a). The relaxed structure shows multiple bent graphene sheets along $[\bar{1}10]$. The bending orientation is that of a carbon nanotube of the (n,n) type, known as the armchair tube.[27,28] The bending radius of the sheets is about 3 Å, which corresponds to a (4,4) tube, illustrated in Fig. 7(c). Nanotubes as small as this are energetically in competition with flat graphene sheets. However, tubes with diameters as small as 5 Å have been observed recently.[29]

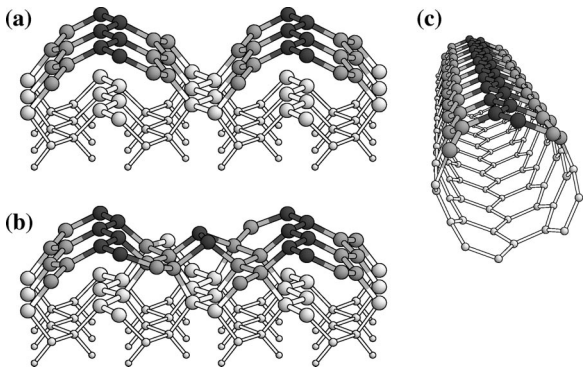

FIG. 7. (a) Graphitization on a 50% covered diamond (110) surface in (2×1) reconstruction, and (b) induced rebonding after deposition of C_2. Dark, gray, and white atoms indicate atoms in the top three monolayers, which are also shown larger than the remaining atoms. The bottom monolayer is the hydrogen termination. (c) For comparison, a (4,4) single-wall carbon nanotube with similar structure and atom designation as (a).

The structural similarity of the bent graphene sheet to a single-wall carbon nanotube allows us to deduce the electronic structure of the bent sheet. The common feature between the bent sheets and the armchair tubes is an atomic zigzag chain of carbon atoms running parallel to the bending axis. Atoms contributing to these chains are sp^{2+x} hybridized, with $x=0$ for flat graphene and $0<x\ll1$ for nanotubes. Along either chain, the overlap of carbon p orbitals normal to the sheet and tube wall, respectively, results in an extended π-bonded system which forms a one-dimensional band. This band has a negligible gap because we find here that Peierls distortion does not occur, quite similar to the situation in armchair nanotubes.[28] Therefore, the atomic and electronic structure will be susceptible to distortions that break the symmetry.

The question of stability of the bent sheets and therefore the diamond surface itself during growth naturally arises. It is known that graphitization on clean diamond surfaces, namely, on (111) and near (111) twin boundaries, leads to delamination.[30,31] We find for the present configuration that it is stable and does not debond. Furthermore, continued adsorption of C_2 in the valley between two arches is possible without a barrier and, more importantly, it causes the sp^2-like atoms near the adsorbate to return to an sp^3 configuration and rebond in the diamond structure, as is illustrated in Fig. 7(b).

Considering the electronic structure of the sheet, we can deduce the reason for the rebonding. Clearly, an approaching dimer will lead to a disturbance of the π-electron system near the graphene sheet. Furthermore, at the terminus of the graphene sheets near the surface, the π-electron system is imperfect to begin with because sp^2-hybridized atoms of the sheets are bonded to sp^3-hybridized, fourfold coordinated atoms at the diamond surface. Since ideal sp^2- and sp^3-hybridized carbon atoms are energetically close, as the cohesive energies of graphite and diamond indicate, the re-

TABLE III. The diffusion barriers E_{barr} and the change in total energy along the diffusion path. The low energy barriers (rows 4 and 5) are associated with the diffusion of a vertically aligned C_2 on top of a C_{2n} cluster.

Path	E_{barr} (eV)	$(E_{final}-E_{init})$ (eV)
C_2 along valley	3.8	0.0
C_2 to other valley	3.3	0.0
C_2 to C_4 along $\rightarrow C_6$	3.7	−1.8
C_2 to end of $C_6 \rightarrow C_8$	1.0 [a]/0.6 [b]	−3.7
C_2 to side of $C_6 \rightarrow C_8$	1.0 [a]/0.6 [c]	−3.1

[a]Near center of C_6.
[b]Near end of C_{2n}.
[c]From metastable state to final energy minimum.

bonded sp^3-hybridized configuration will be lower in energy than the disturbed sp^2 system near the C_2 molecule.

We thus reach the important conclusion that, in the C_2 growth regime established here, intermediate graphitization may occur, but the diamond growth process is stabilized against extended graphitization and delamination.

V. SURFACE DIFFUSION OF C_2

In order to estimate the influence of surface diffusion of C_2 on the growth mechanism, we investigated some diffusion paths, as summarized in Table III. The associated diffusion barriers along the various C_2-related diffusion paths are shown in the second column of this table, and the gain in energy in the last column.

Generally, on the clean diamond (110) surface, the diffusion barriers are rather high, and exceed 3 eV (Table III, rows 1–3). This is easily understood from the strong covalent bond that is formed between a C_2 adsorbed species and the surface once the molecule reaches the surface. The only exceptions to such high barriers are for sites above existing adsorbates, where the binding energy for further adsorbed species is low to begin with. C_2 has the lowest diffusion barriers when it starts diffusion on top of an existing C_{2n} complex. In this case, the barrier for diffusion along the adsorbate ridge is of the order of 1 eV. The C_2 remains nearly vertically oriented, with one of its atoms bonded to one or two surface atoms throughout the diffusion path. The energy barriers are decreasing when the chain end is approached. The last energy barrier toward completing a chain addition step is only 0.6 eV.

We note that the energy gain attainable for a C_2 molecule by diffusion to the end of an existing C_{2n} adsorbate is considerable (see Table III, last column). These gains, when added to the adsorption energies found for the ''top'' deposition sites, as listed in Table II, naturally result in the same total adsorption energies as those for the ''end'' sites. We have thus found two different growth channels, converging to the same growth mechanism. One is adsorption-dominated growth on nearly clean surfaces with deposition directly into diamond lattice sites, and the other is diffusion driven on surfaces densely covered with adsorption clusters.

In the diffusion studies, we found that when the C_2 is directed in either major diffusion direction, along the chain direction of C_{2n} or perpendicular to it, it passes metastable minima before reaching the lowest energy configurations at the chain ends. Along the parallel diffusion path, the last metastable minimum consists of a C_2 fragment singly bonded to the surface, similar to the configuration shown in Fig. 4(b). For the perpendicular direction away from the chain axis toward a neighboring surface valley, the metastable minimum is such that the C_2 atoms complete a fivefold ring, with each one being singly bonded to the surface.

While both intermediate and final diffusion barriers are incidentally the same for diffusion parallel and orthogonal to the C_{2n} chain direction, the ultimate energy *gain* is higher by 0.6 eV for the growth-favoring parallel diffusion; this indicates high adsorption rates in either case, with a preference toward cystalline growth. However, the introduction of defects is quite easily possible under this regime, which helps to explain the rather small grain size found in the final material.

VI. MOLECULAR DYNAMICS DEPOSITIONS

Inspired by the adsorption and diffusion results discussed above we simulated the deposition of C_2 on top of a C_6 complex on the surface directly using molecular dynamics (MD), though within a rather short time span of just 0.1–0.5 ps. The time step in the MD simulations was 10 a.u., i.e., 0.24 fs, and the surface atoms (but not the deposited C_2) were coupled to a heat bath at 1000 K by scaling their velocities with a probability of 0.1 per time step. All the atoms except the terminating hydrogen atoms on the bottom of the surface slab were allowed to follow the Newtonian equations of motion. The goal of these runs was to investigate a diamond growth reaction as follows:

$$C_2^{gas} + C_{2n}^{surf} \rightarrow C_{2n+2}^{surf}. \quad (1)$$

In a first set of experiments, each molecule was initially aligned orthogonal to the surface and shot with a kinetic energy of 2–9 eV along the direction of the $[\bar{1}10]$ surface chains at an angle of 80° to the surface normal vector. The motivation of this particular choice was that the molecule may get adsorbed at the lowest energy position at the end of a C_{2n} cluster, as identified in the diffusion studies. The molecules with up to 7 eV kinetic energy resulted in a C_2 fragment on top of a C_{2n} cluster, similar to the structure in Fig. 4(b). At 9 eV kinetic energy the molecule was deflected from the C_{2n} cluster but was subsequently adsorbed as a lone C_2 on a neighboring clean surface site. While the deflection at higher impact energy seems counterintuitive at first sight, it must be recalled that the incident angle is high, so that the nature of the process is rather one of a steady dissipation of kinetic energy from the approaching C_2 into the substrate until the molecule is slowed down enough to be deposited.

In a second set of runs, a C_2 was aligned parallel to the surface with an initial kinetic energy of 0.1–2 eV and a starting position on top of a C_6 cluster. This leads again to the C_2 fragment being singly bonded to the C_6 surface cluster, a configuration from which diffusion to either end is

possible, as established before. There is a small region above the edge of a C_{2n} ($n=2,3$) cluster, from where a C_2, if given an initial velocity toward the surface, can bond to the metastable minimum that precedes the diamond position, shown in Fig. 5. However, in the molecular dynamics simulations the barrier toward growth completion is too high on our time scale, and we obtained solely the metastable minimum.

VII. SUMMARY AND CONCLUSIONS

We have simulated diamond growth steps by successive deposition of C_2 molecules onto a diamond (110) surface. We find that the initial C_2 adsorption onto a clean (110) diamond surface proceeds with small barriers (0.1–0.2 eV) into the diamond lattice site. The growth mechanism and energetics of this insertion are similar to those on hydrogenated surfaces, as suggested previously.[14] Subsequent C_2 additions on and around the initial adsorbate preferably lead to C_{2n} chains forming along the $[\bar{1}10]$ direction on the surface. The adsorption energies, as listed in Table II, are in the range of 7–10 eV per C_2 molecule at adsorption sites that lead to chain growth, and slightly smaller, 5–7 eV, for sites leading to defected growth. Some backbonds at the C_{2n} chains are broken, leading to a graphenelike morphology, if 50% coverage is reached for the added monolayer. However, the surface remains stable at this point. If the C_2 deposition continues, it induces healing of the broken backbonds due to reformation of sp^3 bonds at the terminus of the graphene sheets.

We also find some metastable C_2 defects during the growth, which may be responsible for starting new nucleation sites, a tendency that would explain the rather small grain size in the experimental studies that motivated this work. Low energy growth may be possible, if the approaching molecule has a kinetic energy within a window of 3–5 eV in order to overcome barriers and avoid defect formation. Direct adsorption into a diamond lattice position is possible only at the end of a C_{2n} cluster or onto a clean site of the surface. Upon coalescence of different C_{2n} chains, the remaining vacancies can be filled by the same growth species, although with slightly higher barriers (0.3–0.6 eV) than in the initial stages.

We have also carried out surface diffusion studies. Because the C_2 adsorptions normally result in tightly bonded adsorbate structures, interisland diffusion of C_2 molecules is rather unlikely. However, an intraisland diffusion path exists, where an added C_2 molecule diffuses on top of a C_{2n} chain until it reaches its end and is incorporated there. This diffusion behavior supports the C_2 addition model that was evident from the deposition energetics. An implication of this fact is that an enhancement of surface diffusion rates would result in an increase in growth rate, by virtue of diffusion of migrating C_2 species to and eventual incorporation into growth sites.

ACKNOWLEDGMENTS

This work was carried out with the support of Helsinki University of Technology, The Center for Scientific Computing in Finland, and the Deutsche Forschungsgemeinschaft. One of the authors M.S. is grateful to D. M. Gruen and G. Seifert for many fruitful discussions.

*Electronic address: sternberg@phys.uni-paderborn.de

[1] D.M. Gruen, S. Liu, A.R. Krauss, J. Luo, and X. Pan, Appl. Phys. Lett. **64**, 1502 (1994).

[2] C. Zuiker, A.R. Krauss, D.M. Gruen, X. Pan, J.C. Li, R. Csencsits, A. Erdemir, C. Bindal, and G. Fenske, Thin Solid Films **270**, 154 (1995).

[3] H.-G. Busmann, U. Brauneck, and H.-W. David, Carbon **36**, 529 (1998); in *Fullerenes and Carbon Based Materials*, edited by P. Delhaes and H. Kuzmany, European Materials Research Society Symposium Proceedings No. 68 (Elsevier Science SA, Lausanne, 1998), p. 529.

[4] D. Zhou, D.M. Gruen, L.-C. Qin, T.G. McCauley, and A.R. Krauss, J. Appl. Phys. **84**, 1981 (1998).

[5] A.N. Goyette, Y. Matsuda, L.W. Anderson, and J.E. Lawler, J. Vac. Sci. Technol. A **16**, 337 (1998).

[6] T. Lin, G.Y. Yu, A.T.S. Wee, Z.X. Shen, and Kian Ping Loh, Appl. Phys. Lett. **77**, 2692 (2000).

[7] A. Erdemir, M. Halter, G.R. Fenske, R. Csencsits, A.R. Krauss, and D.M. Gruen, Tribol. Trans. **40**, 667 (1997).

[8] A. Erdemir, C. Bindal, G.R. Fenske, C. Zuiker, R. Csencsits, A.R. Krauss, and D.M. Gruen, Diamond Films Technol. **6**, 31 (1996).

[9] P. Keblinski, D. Wolf, S.R. Phillpot, and H. Gleiter, J. Mater. Res. **13**, 2077 (1998).

[10] Michael Sternberg, Peter Zapol, Thomas Frauenheim, Dieter M. Gruen, and Larry A. Curtiss, in *Amorphous and Nanostructured Carbon*, edited by J. Robertson, J.P. Sullivan, O. Zhou, T.B. Allen, and B.F. Coll, Mater. Res. Soc. Symp. Proc. No. 593 (Materials Research Society, Pittsburgh, 2000), p. 483.

[11] D. Zhou, A.R. Krauss, T.D. Corrigan, T.G. McCauley, R.P.H. Chang, and D.M. Gruen, J. Electrochem. Soc. **144**, L224 (1997).

[12] C.J. Chu, R.H. Hauge, J.L. Margrave, and M.P. D'Evelyn, Appl. Phys. Lett. **61**, 1393 (1992).

[13] D.A. Horner, L.A. Curtiss, and D.M. Gruen, Chem. Phys. Lett. **233**, 243 (1995).

[14] P.C. Redfern, D.A. Horner, L.A. Curtiss, and D.M. Gruen, J. Phys. Chem. **100**, 11 654 (1996).

[15] G. Ciccotti, M. Ferrario, and J.-P. Ryckaert, Mol. Phys. **47**, 1253 (1982).

[16] J.-P. Ryckaert, Mol. Phys. **55**, 549 (1985).

[17] J.M. Thjissen, *Computational Physics* (Cambridge University Press, Cambridge, 1999), pp. 218–220.

[18] D. Porezag, Th. Frauenheim, Th. Köhler, G. Seifert, and R. Kaschner, Phys. Rev. B **51**, 12 947 (1995).

[19] M. Elstner, D. Porezag, G. Jungnickel, J. Elsner, M. Haugk, Th. Frauenheim, S. Suhai, and G. Seifert, Phys. Rev. B **58**, 7260 (1998).

[20] Th. Frauenheim, G. Jungnickel, P. Sitch, M. Kaukonen, F. Weich, J. Widany, and D. Porezag, Diamond Relat. Mater. **7**, 348 (1998).

[21] M. Kaukonen, P.K. Sitch, G. Jungnickel, R.M. Nieminen, Sami Pöykkö, D. Porezag, and Th. Frauenheim, Phys. Rev. B **57**, 9965 (1998).

[22] Th. Köhler, Th. Frauenheim, and G. Jungnickel, Phys. Rev. B **52**, 11 837 (1995).
[23] B.N. Davidson and W.E. Pickett, Phys. Rev. B **49**, 11 253 (1994).
[24] D.R. Alfonso, D.A. Drabold, and S.E. Ulloa, Phys. Rev. B **51**, 14 669 (1995).
[25] G. Kern and J. Hafner, Phys. Rev. B **56**, 4203 (1998).
[26] S.C. Lim, R. E. Stallcup II, I. Akwani, and J.M. Perez, in *Materials Issues in Vacuum Microelectronics*, edited by W. Zhu, L. S. Pan, T. E. Felter, and C. Holland, Mater. Res. Soc. Symp. Proc. No. 509 (Materials Research Society, Pittsburgh, 1998), p. 165.
[27] R. Saito, M. Fujita, G. Dresselhaus, and M.S. Dresselhaus, Appl. Phys. Lett. **60**, 2204 (1992).
[28] J.W. Mintmire, B.I. Dunlap, and C.T. White, Phys. Rev. Lett. **68**, 631 (1992).
[29] L.-M. Peng, Z.L. Zhang, Z.Q. Xue, Q.D. Wu, Z.N. Gu, and D.G. Pettifor, Phys. Rev. Lett. **85**, 3249 (2000).
[30] G. Jungnickel, D. Porezag, T. Frauenheim, W.R.L. Lambrecht, B. Segall, and J.C. Angus, in *Mechanical Behavior of Diamond and Other Forms of Carbon*, edited by M. D. Drory, M. S. Donley, D. Bogy, and J. E. Field, Mater. Res. Soc. Symp. Proc. No. **383** (Materials Research Society, Pittsburgh, 1995), p. 349.
[31] V.L. Kuznetsov, I.L. Zilberberg, Y.V. Butenko, A.L. Chuvilin, and B. Segall, J. Appl. Phys. **86**, 863 (1999).